Micro ring resonators as building blocks for an all-optical high-speed reservoir-computing bit-pattern-recognition system

Charis Mesaritakis,* Vassilis Papataxiarhis, and Dimitris Syvridis

National and Kapodistrian University of Athens, Department of Informatics & Telecommunications, Panepistimiopolis Ilisia 15345, Athens, Greece
**Corresponding author: cmesar@di.uoa.gr*

Received July 17, 2013; revised October 2, 2013; accepted October 2, 2013; posted October 3, 2013 (Doc. ID 193099); published October 31, 2013

In this paper, an alternative approach for an integrated photonic reservoir computer is presented. The fundamental building block of the reservoir is based on the nonlinear response of a ring resonator, where effects such as two-photon absorption and nonlinear refractive index variation were taken into consideration. In order to investigate the validity of this scheme, the response of a single add/drop micro ring was simulated through a traveling wave numerical model, and the parameters that affect the nonlinearity of the response were identified. Based on these results, a 5×5 matrix of randomly interconnected resonators was utilized in order to classify different high-bit-rate digital patterns. Simulations confirmed that the proposed system could offer a classification error of 0.5% for bit rates up to 160 Gbps and for 8-bit-length digital words.

OCIS codes: (170.0110) Imaging systems; (170.3010) Image reconstruction techniques; (170.3660) Light propagation in tissues.
http://dx.doi.org/10.1364/JOSAB.30.003048

1. INTRODUCTION

A newly emerging scientific area is the photonic implementation of traditional computer-based computational tools such as neural networks [1]. Such application can provide all-optical artificial intelligence in optical networks and subsystems and thus eliminate the need for costly electro-optic conversions, radically increase computation speed, and enhance the operational capabilities of optical systems [2–6]. The major obstacle with such an approach is the fact that typical neural networks (optical or conventional) are static implementations and cannot be used to predict time-dependent signals, which is a highly desired feature in state-of-the-art communication systems. An alternative is the use of recurrent neural network topologies, [7,8] but, although they can be transferred in the optical domain, the algorithmic training of such schemes is cumbersome [9].

The pattern-recognition community bypassed this limitation and proposed a novel approach called reservoir computing. In this approach, a computational block that consists of a complex interconnection of nonlinear (usually sigmoid) neurons with feedback loops is used, whose weights remain random and untrained. This block is followed by a simple feed-forward neural network (perceptron) without feedback loops, which classifies the time-series [Fig. 1(a)] [10,11]. By using this approach, the neural-network training problem is limited only in the perceptron section, and thus it can be performed efficiently with typical back-propagation training algorithms. A simplified explanation of the operating principle of a reservoir is that the high complexity and nonlinear response of the reservoir neurons increases the dimensionality of the classification problem thus makes the different signals more distinguishable by a trained simplified neural network.

Using this concept, many software/electronic-based reservoirs have been realized for applications such as event-driven response in robotic systems [12,13], chaotic time series prediction [10], real-time voice recognition [14,15], and epileptic seizures identification [16]. Nonetheless, these implementations lack the high-speed and low-power-consumption capabilities present in photonic devices. In the pioneer work of [17], a photonic implementation of a reservoir computer was proposed, where, instead of the typical sigmoid function, the input/output optical power response of a semiconductor optical amplifier (SOA) was used as the nonlinear element of the reservoir. This photonic implementation surpassed the conventional computer-based solution in a simple classification problem that consisted of distinguishing triangular and square optical pulses. The same group applied the concept of optical-reservoir computing into various fields, whereas they also demonstrated a unified simulation tool for the implementation of various photonic circuits (photonic crystals, lasers, etc.) as building blocks for various dynamical systems [18].

More recently, another group applied successfully an alternative concept for a photonic reservoir that consisted of only one nonlinear element (Mach–Zehnder interferometer); thus simplifying the hardware requirements for the realization of such a system [19–21]. In this case an opto-electronic feedback scheme at the edge of stability was utilized, whereas the different outputs of the reservoir were acquired through different optical couplers from a 4 km optical fiber. Through this approach, promising results concerning the real-time identification of spoken digits have been acquired.

Based on the observation of the aforementioned groups that the nonlinear response of each reservoir's neuron could be different from the traditional sigmoid function, we propose an alternative approach, where the nonlinear response of an interconnected matrix of micro ring resonator (MRR) add/drop filters [Fig. 1(b)] is used in order to utilize a fully functional reservoir computing system. In detail, the MRRs can provide power-dependent nonlinear responses if effects such as two-photon-absorption (TPA) and nonlinear refractive index variation are taken into consideration. In order to validate our approach, we have used a traveling wave numerical model in order to investigate the nonlinear response of a single add/drop InGaAsP/InP MRR versus input power, whereas the MRR's structural characteristics that affect the degree of the nonlinearity were also examined.

Furthermore, a 5×5 MRR matrix with random delays/feedback loops and a rainfall topology was simulated using the aforementioned model [Fig. 1(c)]. Its capability to classify different 3- and 8-bit non-return-to-zero (NRZ) patterns was tested for different pulse-extinction ratio and signal-to-noise ratio (SNR). The results confirmed that the proposed scheme is able to classify different 8-bit digital words with a bitrate of 160 Gbps and with a mean square error of 0.5%. Moreover, the aforementioned promising results alongside the high integration capabilities, low power consumption, and ultra-fast response time offered by

$$\frac{\vartheta A}{\vartheta z}=\left[-\frac{\alpha}{2}\right]\cdot A+\left[-\frac{\beta}{2\cdot A_{\text{eff}}}+j\cdot\gamma\right]\times A+\left[\frac{-N_f\cdot\sigma_\alpha}{2}+j\frac{\omega\cdot\sigma_\alpha\cdot N_f}{c}\right]\cdot A, \tag{1}$$

$$\frac{\partial N_f}{\partial t}=\frac{\beta}{2\hbar\omega\cdot A_{\text{eff}}^2}\cdot P^2-\frac{N_f}{\tau_{\text{ph}}}, \tag{2}$$

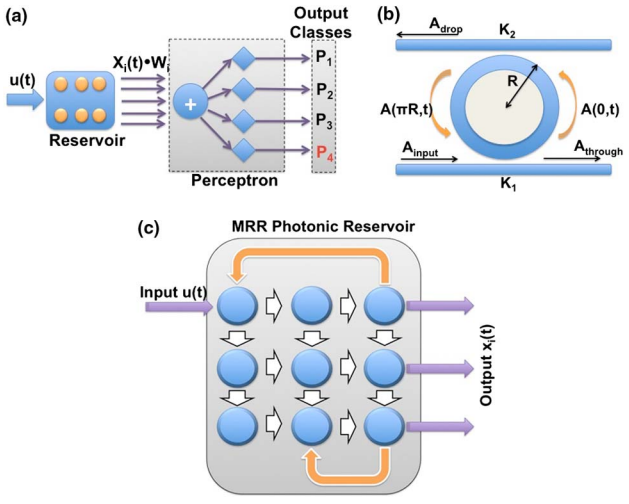

Fig. 1. (a) Basic schematic of a photonic reservoir computing system followed by a simple perceptron. $u(t)$ corresponds to the time-dependent input and $x_i(t)$ to the reservoir outputs, whereas W_i are the trainable weights, finally $P_{1\text{–}4}$ are the final classification results. (b) Basic schematic of an add/drop MRR, where A_{input} corresponds to the system input, and A_{through} and A_{drop} are the two outputs. In our case, no add signal is utilized. (c) Rain-fall topology of the MRR-based reservoir with various feedback loops. First MRR in the matrix is the input, while the last column provides five outputs.

$$A(0,t)=-jkA^{\text{in}}(t)+\tau\cdot A(2\pi R,t)\cdot e^{-j2\pi kR}, \tag{3a}$$

$$A(\pi R,t)=-jk\cdot A_{\text{add}}(t)+\tau\cdot A(\pi R,t)e^{-j\pi nkR}, \tag{3b}$$

$$A_{\text{thr}}(t)=\tau\cdot A^{\text{in}}(t)-jk\cdot A(2\pi R,t)\cdot e^{-j2\pi nkR}, \tag{3c}$$

$$A_{\text{drp}}(t)=-jk\cdot A(\pi R,t)\cdot e^{-j\pi nkR}. \tag{3d}$$

MRRs, can allow the hardware implementation of such a scheme in various applications such as all-optical routers or high-bit rate digital-to-analog converters.

2. SINGLE MRR MODEL AND SIMULATIONS

The MRRs provide significant advantages due to their ultra-small dimensions and their facet-free high-finesse resonances. Based on these advantages, many applications have benefited from MRRs such as high-quality filters [22,23], bio-chemical sensors [24], miniature MRR lasers [25], sparkling neurons [26], and ultra-fast logic gates [27]. Especially in the last case, the MRR's operation had been modeled through a traveling wave approach, where nonlinear effects such as TPA and nonlinear refractive index variations have been taken into consideration [27]. Our approach is based on the same model and the basic equations used are Eqs. (1)–(3), where A is the slow varying envelope of the optical field, N_f is the time-varying free-carrier concentration, P is the total optical power, α is the linear absorption coefficient, and β is the nonlinear TPA coefficient, $\gamma=n_2\omega/A_{\text{eff}}c$, with n_2 and A_{eff} being the nonlinear refraction coefficient and the waveguide effective area, respectively. The parameters σ_α and σ_r are the free carrier absorption cross-section and the refractive index change per carrier per density, triggered by the TPA. Finally, by taking into consideration that κ, τ are the coupling and transmission coefficients, respectively, whereas R corresponds to the ring radius, Eqs. (3a)–(3d) represent the basic equations for the calculation of the optical field at the through and drop port. The parameters used in simulations are presented in Table 1.

In our simulations, we have assumed a single add/drop MRR with a radius of 50 μm with losses equal to 10 cm^{-1}, while the coupling coefficient was set to $k=0.1$ ($k_1=k_2$) symmetric for both ports (through/drop) [Fig. 1(b)]. In Fig. 2(a), the transfer function of the through port has been computed through the traveling wave model by varying the central frequency of the input field by 50 GHz relative to the resonance of the MRR for different levels of optical power. It can be observed that, due to the increased intracavity power, the TPA effect reduces the optical power, whereas due to the nonlinear dependence of the refractive index, the MRR's central resonance is shifted, and the response becomes asymmetric. According to the same principle, the increased power inside the cavity also affects the transfer function of the drop port [Fig. 2(b)].

From Fig. 2, it can be concluded that if the frequency of the input signal is kept constant, and input optical power is varied, then a nonlinear power variation will occur at the MRR's outputs, due the frequency shift of the through and drop port response. In particular in Fig. 3(a), the output power for both outputs (through and drop) is plotted versus different levels

Table 1. MRR Simulation Parameters

Parameter	Symbol	Value
Nonlinear refractive coefficient	n_2 (m^2/W)	1.4×10^{-16}
Waveguide effective area	A_{eff} (μm^2)	0.25
Nonlinear TPA coefficient	B (cm/GW)	33.3
Free carrier absorption cross section	σ_a (cm^2)	1.5×10^{-16}
Refractive index change per carrier	σ_r (cm^3)	-1×10^{-20}
Carrier relaxation time	τ_{ph} (ps)	100
Group refractive index	n	3.3

of input power for input frequency matching the MRR's resonance and for the same MRR parameters as in Figs. 2(a) and 2(b).

By comparing the input–output power response, it can be observed that for the through port, the function is almost linear. This stems from the fact that the increased input power in the MRR shifts the MRR's resonance; thus the notch filter capabilities of the through port are degraded. Consequently, the output power increases almost linearly with input, and this port's response cannot be utilized efficiently as a building block for a reservoir system. On the other hand, the drop port's response is also affected by the transfer function of the through port, and thus it exhibits more complex behavior.

Nonetheless, the nonlinearity observed in this case varies significantly compared to the SOA approach utilized in the past [17]. The difference between the SOA and the MRR response resides to the fact that for high input power ($P_{in} > 10$ mW), the optical power in the MRR is not saturated, but it continues to increase linearly due to the strong frequency detuning of both ports. Moreover, the MRR's response is different also from the sigmoid transfer function, which is step-like. Taking into consideration the fact that the level of nonlinearity in each neuron is of crucial important to the reservoir's performance, the MRR's structural parameters that affect the drop port's response are investigated. In this case, the input signal frequency is kept constant in order to coincide with one of the MRR's resonances ($\lambda = 193.8154$ THz), while the input power varies from 1 μW to 10 mW.

The first parameter to be considered is the ring radius. In Fig. 3(b), the drop port power is computed versus the input power for an MRR with linear losses of 200 cm^{-1} and $k = 0.1$, while the ring radius varies from 5 to 45 μm. It can be seen that as the ring radius increases, the system's response is more linear. This effect originates from the fact that the circumference of the ring ($L = 2\pi R$) increases, thus the internal losses are enhanced. This reduction in the intracavity optical power suppresses TPA related effects and reduce nonlinearity. The same effect can be monitored if the ring radius is kept constant at $R = 45$ μm ($k = 0.1$) while the linear losses vary from the lossless case of 1 cm^{-1} to increased material losses of 200 cm^{-1} [Fig. 3(c)].

Regarding the role of coupling efficiency (k) to the response of the MRR, the output power versus the input power for a MRR of $R = 10$ μm and $\alpha = 10$ cm^{-1} is computed for a coupling efficiency (k) that varies from 0.1 to 0.3 [Fig. 3(d)]. It can be seen that for high values of k ($k > 0.2$), the system exhibits linear response. This effect can be attributed to the equivalence of coupling efficiency of the MRR to the reflectivity of a classical Fabry–Perot cavity. As k decreases, the Q factor of the notch-filter (through port) increases; thus if the injected field is in resonance with the cavity, an increased amount of optical power will lock inside the cavity. The cavity enhancement will increase the TPA effects; thus it will also enhance the nonlinearity in the response.

Summarizing the aforementioned simulation results, the highest nonlinearity at the drop port manifests for small round-trip losses that can be triggered either from reduced ring radius or suppressed propagation losses, whereas high nonlinear response can be also achieved in case the MRR cavity is considered critically coupled [28,29]. In a practical way, these guidelines can be achieved through various approaches. Utilization of active materials for the fabrication of the cavity can allow limited electrical pumping that will enable loss minimization or tuning [30]. Furthermore, by taking into consideration the trade-off between the bending losses and propagation losses, due to increased circumference, the MRR can be designed in order to exhibit increased nonlinear response even in the absence of any loss-compensation scheme. For example, a ring radius of 5 μm and $a = 100$ cm^{-1} depending on the k can offer increased nonlinear behavior. Last, in order to tune the coupling efficiency, either precise fabrication techniques could be employed that can set the coupling efficiency within a reasonable deviation or MEM/thermal tunable couplers could be integrated inside the MRR aiming to fine-tune the coupling efficiency [31].

Furthermore, it is worth mentioning that due to the high finesse attained by such schemes, even minor power variations at the MRR's input induce significant spectral shifts that enhance the nonlinear response. On the other hand, in

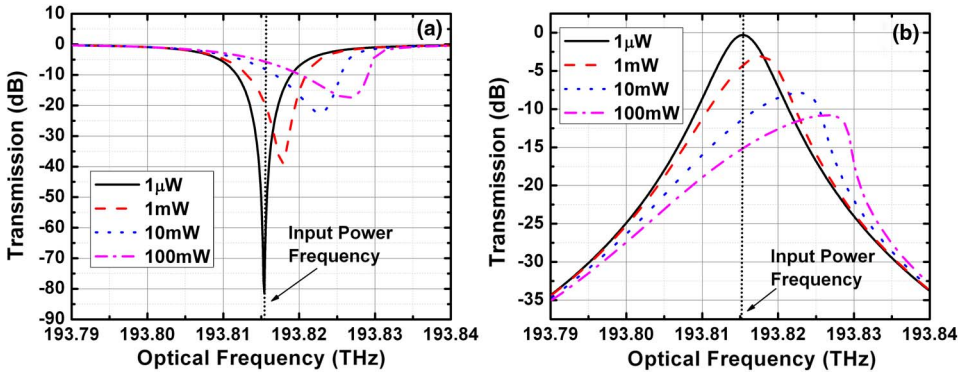

Fig. 2. (a) Through-port transfer function of a single MRR with various input power ranging from 1 μW to 100 mW. (b) Drop-port transfer function for the same input power range.

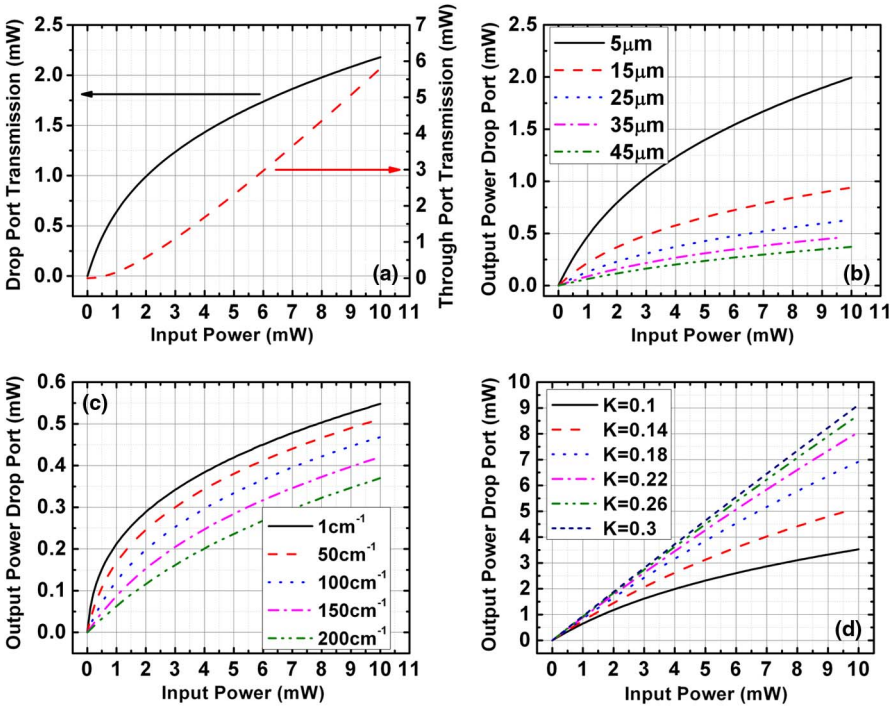

Fig. 3. Drop output power versus input for various cases. (a) Power response of both ports for the structural parameters used in Fig. 2. (b) Radius investigation for losses = 200 cm^{-1} $k = 0.1$. (c) Losses investigation for $R = 45$ μm, $k = 0.1$. (d) Coupling investigation for $R = 10$ μm and $\alpha = 10$ cm^{-1}.

case the input power is high ($P_{in} > 10$ mW), the frequency detuning at the through port is strong enough to diminish any nonlinear response. Consequently, nonlinearity can be triggered by low power variations, allowing the use of a complete passive scheme with zero electrical demands.

3. MRR MATRIX FOR RESERVOIR COMPUTING

Based on the aforementioned results, an add/drop MRR was utilized as a building block for a reservoir computing system. In detail, a matrix of 25 MRRs has been modeled using the aforementioned traveling wave approach. The MRRs were interconnected using a rainfall topology similar to [17,18], where each MRR's input was provided through the drop port of the previous MRR [Fig. 1(b)]. The time delay between each MRR was set randomly from a uniform distribution process and ranged from 50 fs to 4.5 ps that correspond to an optical waveguide length of 4.3 μm and 0.4 mm, respectively (assuming group refractive index of 3.3).

The first MRR in the matrix was assumed to be the input of the system, while the MRRs at the last column of the matrix were utilized as five discrete system outputs. A subset of the 25 MRRs was randomly chosen to have additional feedback loops from the outputs of the system with additional random delays. Finally, the coupling strength between the MRRs and in the feedback loops was also randomly chosen. Nonetheless, all coupling strength values were set below 1. This condition has been chosen so as to suppress chaotic behavior that could hinder the deterministic nature of the computation [17–19]. Furthermore, in order for the reservoir to operate efficiently, it should exhibit a "fading memory" effect, meaning that after a predicative point of time the system should return to its initial condition. In order to achieve this, the MRRs were not considered lossless, and, as mentioned above, the coupling strength of the MRRs was set below 1. For the sake of simplicity in these simulations, all MRRs were considered identical with an $R = 5$ μm, losses in the order of 100 cm^{-1}, and coupling efficiency of $k = 0.1$. Through utilization of identical MRRs, it is implied that their spectral resonances coincide. This effect cannot be achieved in a real system due to random fabrication deviations at the structural characteristics of each MRR. Nonetheless, the assumption made in this paper does not compromise the generality of the scheme, due to the fact that a variation in the wavelength of the resonance results to reduced coupling of optical power between MRRs, and this effect has been included in the computations through the use of reduced coupling strength between MRRs.

In order to prove the capabilities of the aforementioned scheme, a simple classification problem was considered. Four 3-bit digital words encoded as simple optical NRZ pulses were fed to the reservoir at a bit rate of 40 Gbps. The time-dependent outputs of the optical reservoir were fed to a perceptron whose weight was trained using typical back-propagation algorithms. In Fig. 4, typical reservoir outputs are presented for four characteristic digital words. It is worth mentioning that the reservoir does not operate as a simple integrator. This can be confirmed by the fact that two used digital words (101 and 110) correspond to the same amount of optical power at the system's input, but result to different optical power at the output.

Furthermore, the reservoir exhibits a time delay in producing an output for each case. This delay corresponds to the internal delays in the MRR's connections in the employed topology and in the feedback loops. The reservoir delay is directly related to the length of the digital word that the system

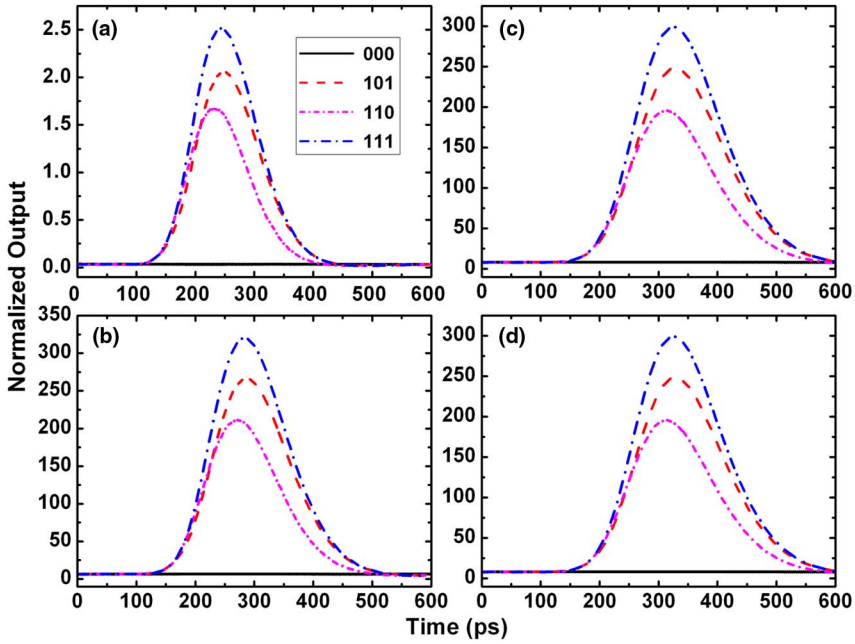

Fig. 4. (a)–(d) Time series produced from four different reservoir outputs for four discrete digital words (000, 101, 110, 111).

attempts to discriminate. In detail, the reservoir-induced time delay should exceed the time period of the word, so as to store the entire bit stream and be able to produce different outputs, even in the case that two words differ only in the most/least significant bit (first to arrive). In this case, the maximum MRR delay is 4.5 ps, whereas due to the rainfall architecture, the MRR delay, and the feedback loops the final delay was in the order of 80 ps. Taking into consideration the above-mentioned discussion, the system can support and classify longer words (8 or 16 bit) by either increasing the length of the interconnecting optical waveguides, and thus increase the reservoir's memory, or by simply increasing the bit rate.

Furthermore, in order to investigate the system's performance for various input conditions, we considered two distinctive cases. In both cases, the extinction ratio (P_1/P_0), where P_1 and P_0 correspond to the optical power of "1" and "0" bit, respectively, varied from 3 to 10 dB. This was achieved by varying P_0, while P_1 was kept constant at 10 or 100 mW [Figs. 5(a)–5(c)]. Moreover, so as to create a set of plausible real-life conditions, we varied the SNR by using an optical amplifier's gain [erbium-doped fiber amplifier (EDFA)], so as to keep the input power of the reservoir constant but with a different level of noise. Through this approach, by increasing the amplifier's gain, the optical power and the extinction ratio at the reservoir's input were kept constant, but the SNR decreased. For each power level and extinction ratio, the time-dependent outputs of the reservoir were fed to a simple perceptron, whose weights were trained using a typical back-propagation algorithm. In our case, 50% of the samples were used as the training set and 20% were used for validation, whereas 30% percent of the samples were utilized as test time series. Through this approach, we calculated for the test time series the total classification error (mean square error) that corresponds to the percentage of time samples for which the perceptron failed to classify correctly the given bit pattern. It is worth mentioning that most errors occur at the system's transition from each bit pattern, while after the transition the perceptron's output presents the correct class.

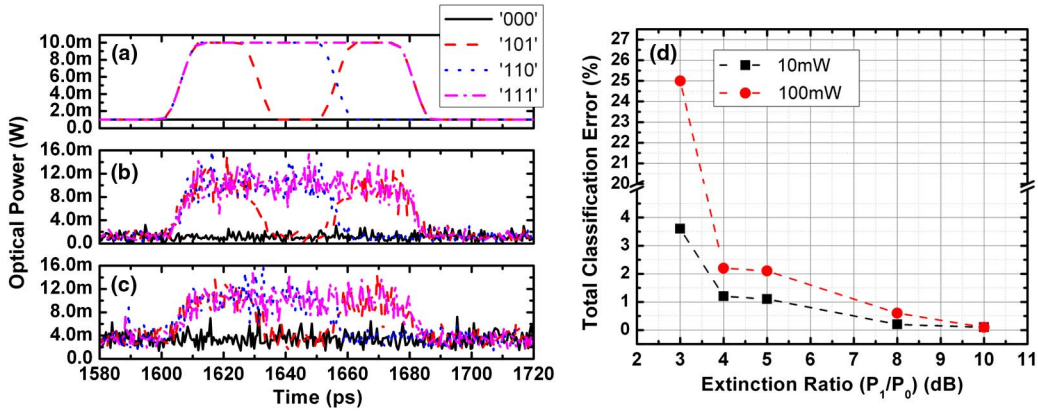

Fig. 5. Optical input for four digital words with $P_1 = 10$ mW. (a) 10 dB extinction ratio noiseless case (0 dB gain). (b) 10 dB extinction ratio 20 dB EDFA gain. (c) 5 dB extinction ratio 20 dB EDFA gain. (d) Total classification error versus the extinction ratio for two cases (black square) correspond to input power of 10 mW (red circles) 100 mW.

In Fig. 5(d), the total classification error for the aforementioned four digital words is computed versus the extinction ratio (P_1/P_0) for two different cases $P_{in} = 10$ mW (black square) and $P_{in} = 100$ mW (red circle). It is worth mentioning that for all cases as the extinction ratio decreases, more errors occur in the system. This effect originates from the fact that "0" and "1" bits have lower power difference and, consequently, cause an almost identical reservoir response. On the other hand, if a higher extinction ratio is employed at the system's input (10 dB), the classification error drops down to 0.1% for both cases. By comparing the two input power cases (10 and 100 mW), it can be seen that in the case that higher optical input is employed, the system exhibits increased error rate compared to the 10 mW case. In particular, for the lower extinction ratio of 3 dB and 100 mW input, the system's computational power significantly degrades exhibiting a classification error of 25%. On the other hand, if the input power is limited to 10 mW, the classification error in the 3 dB extinction ratio case corresponds to an error of not more than 3.5%. The same effect is demonstrated more clearly in Fig. 6, where the total classification error has been computed versus input power for a constant extinction ratio of 3 dB (black squares) and 10 dB (red circles). It can be seen that as input power is reduced, the classification errors degrade, from 25% for $P_{in} = 100$ mW to 1.7% for 5 mW optical input. In this case, that extinction ratio is increased to 10 dB, then the system errors remain low (in the order of 0.1%), and the input power does not impose restrictions in the system's performance.

This effect can be attributed to the regime of operation of the MRR for each case. In detail, if $P_1 = 1$ mW and P_0 varies according to the used extinction ratio, the MRR operates within the nonlinear regime (see Fig. 3), thus the reservoir exhibits increased computational efficiency. On the other hand, if $P_{in} = 100$ mW is considered, the injected optical power is high enough in order to significantly detune the MRR's response in relevance to the input signal and, consequently, offer a more linear operation at each neuron. On the other hand, if the power difference between P_1 and P_0 is high (10 dB), then despite the input power, the operational regime [see Figs. 3(b)–3(d)] is extensive, and a significant level of nonlinearity at each neuron is preserved.

The above results indicate an interesting property of the system related to its nonlinear behavior as a function of input power. In the majority of the physical systems, the nonlinearity appears at relatively high injected-power levels. This would be a severe limitation for a complex raindrop optical topology since the optical power reaching the remote neurons would be low and not sufficient to drive them to the nonlinear regime. On the contrary, in the proposed approach, a strong nonlinearity appears at low levels of optical power resulting in a nonlinear contribution from all elements of the network without electrical or optical pumping schemes.

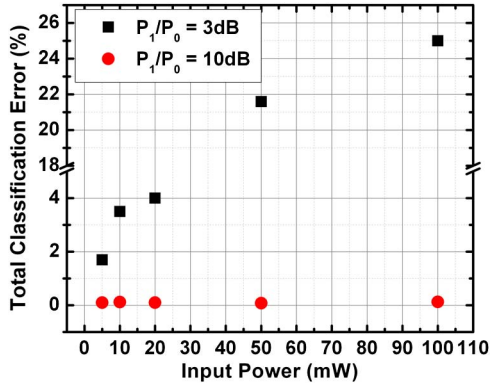

Fig. 6. Total classification error for the aforementioned MRR reservoir versus input power and for a constant extinction ratio of 3 dB (black squares) and 10 dB (red circles).

Finally, in order to further prove the efficiency of the proposed system, an 8-bit training set was created using the same MRR setup as in the previous examples. In this case the bit rate was increased to 160 Gbps, the extinction ratio was kept at 10 dB, whereas the training set consisted of digital patters with varying levels of noise. The perceptron training utilized 50% of the samples as a training set, whereas the rest were used as test patterns, providing a misclassification error of 0.5%. In Fig. 7, a test bit pattern that consists of consecutive 8-bit digital words is presented alongside the response of the perceptron for two cases. The perceptron's output is time dependent, and, for every time frame, each perceptron's output that corresponds to a predetermined digital word (class) has a certain power level. The system's response (classification) is determined by the output with the highest power.

In Fig. 7(a), the bit pattern was amplified through a 5 dB gain amplifier that resulted to a constant 10 mW input power and reduced noise. In Fig. 7(b), the corresponding perceptron classification is presented. In detail, before any bit pattern is

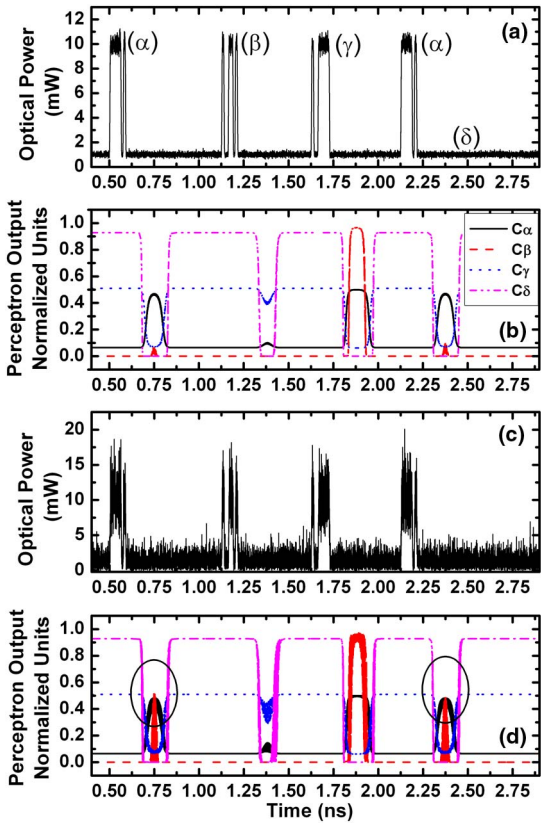

Fig. 7. (a) Time trace of the input bit stream, four different words are used α: "11111010"; β: "10011010"; γ: "10011111"; and δ:"00000000" with an EDFA level of 5 dB. (b) Perceptron output classifiers- C_α, C_β, C_γ, and C_δ, correspond to the α, β, γ, δ bit patterns, respectively. (c) Same as (a) with 20 dB gain form the EDFA. (d) Corresponding classifiers with errors (in circle).

applied at the system, the perceptron's output corresponds to C_δ (this output has the highest power) that corresponds to the digital word "000000000." When the first pattern is applied (α), and after a certain delay the power of all the outputs is reduced (C_β, C_γ, and C_δ), while C_α, which corresponds to the correct pattern, increases. Before the next pattern is applied, the system returns to its initial value (C_δ) and changes again when the next patterns enter the reservoir. It is worth noting that in this case [Fig. 7(b)], the response of the perceptron's offers an error-free detection. On the other hand, in Fig. 7(c) the same bit-stream was used but with increased amplifier gain (20 dB) resulting in increased noise level; consequently, the perceptron's output [Fig. 7(d)] demonstrates in two cases some classification errors. In this case, the bit pattern C_α is applied for some time frames the C_β obtains a higher power. The aforementioned misclassification is marked with a black circle in Fig. 7(d).

Furthermore, it is worth mentioning that the delay observed for the neural network to classify each pattern is the accumulative effect of the real delay (80 ps) imposed by the *memory* of the reservoir and the perceptron's delay (which in this case was realized by a computer software). In this case, that a simple all-optical perceptron is employed (simple optical waveguides with tunable losses), the perceptron-induced delay could be minimized.

4. CONCLUSION

In this paper, an alternative approach for the realization of an all-optic reservoir computer is presented. In our case, the fundamental building block (neuron) for the reservoir is the nonlinear response of an add/drop MRR, which is triggered by nonlinear effects such as TPA and nonlinear refractive index variation in the MRR cavity. Through the use of a traveling wave numerical model, the nonlinear response of a single MRR was investigated, whereas the structural parameters that affect the degree of the nonlinearity were also examined. Based on these results, the optimum parameters were employed on a 5×5 matrix of randomly interconnected MRRs with randomly positioned feedback loops, followed by a simple perceptron. In order to validate the system's performance, a simple classification task was used, which consisted of discriminating 3- and 8-bit NRZ digital words with a 40 and 160 Gbps bit rate, respectively. In both cases, the reservoir computer offered small classification errors of 0.1% and 0.5%, respectively, for a pulse extinction ratio of 10 dB.

The nonlinear transfer function of the MRR, triggered by the TPA and Kerr effect, differs from previous reservoir functions. Nonetheless, it is not anticipated to provide a direct enhancement in the performance of a reservoir-computing scheme, compared to past implementations based on SOAs and Mach–Zehnder interferometers. On the other hand, the existence of significant nonlinear response at each MRR neuron with relative low input power in the absence of any pumping setup can allow energy consumption minimization, whereas it can increase the computational efficiency of the MRR-based reservoir due to the fact that even remote neurons, where the propagation losses can be extensive, provide increased nonlinear response.

The limited size of MRR structures, and the versatility concerning the material system used to realize them, can minimize the final footprint of all-optic reservoirs and drastically reduce the manufacturing cost. In addition, the use of an all-passive photonic reservoir based on MRRs can minimize the system's complexity, significantly reduce fabrication cost, and eliminate thermal effects due to lack of any electrical pumping. Furthermore, MRRs have been used in the past efficiently for high-speed telecomm applications; this fact can allow the use of reservoir-computing setups in new areas such as high bit-pattern recognition in all-optical routers or analog-to-digital converters.

In the case of planar-technology SOA-based reservoirs, optical interconnections cannot cross each other, and, consequently, the reservoir's connection complexity remains limited. On the other hand, by incorporating lateral and vertical coupling schemes for the coupling of MRRs and straight waveguides, multiple inputs and outputs at each neuron can be easily fabricated, thus enhancing the reservoir's complexity and, consequently, its computational strength.

Finally, although a direct comparison between the SOA and Mach–Zehnder approach is beyond the scope of this work, the very low errors observed for a complex classification problem such as 8-bit high bit-rate pattern recognition implies that the low-power nonlinearity observed at MRR-based reservoirs can offer increased computational strength compared to previous implementations.

Finally, in this study, the InGaAsP/InP material system has been considered, but the principle of operation could be easily transferred in a different material as long as effects such as TPA and Kerr are still present to offer a nonlinear response at each neuron.

REFERENCES

1. K. Hornik, M. Stinchcombe, and H. White, "Multilayer feedforward networks are universal approximators," Neural Netw. **2**, 359–366 (1989).
2. D. Psaltis, D. Brady, and K. Wagner, "Adaptive optical networks using photorefractive crystals," Appl. Opt. **27**, 1752–1759 (1988).
3. A. Hurtado, K. Schires, I. D. Henning, and M. J. Adams, "Investigation of vertical cavity surface emitting laser dynamics for neuromorphic photonic systems," AIP Appl. Phys. Lett. **100**, 103703 (2012).
4. K. Kravtsov, M. P. Fok, D. Rosenbluth, and P. R. Prucnal, "Ultrafast all-optical implementation of a leaky integrate-and-fire neuron," Opt. Express **19**, 2133–2147 (2011).
5. B. Javidi, J. Li, and Q. Tang, "Optical implementation of neural networks for face recognition by the use of nonlinear joint transform correlators," Appl. Opt. **34**, 3950–3962 (1995).
6. M. Hill, E. Edward, E. Frietman, H. de Waardt, H. J. S. Dorren, and G. Khoe, "All fiber-optic neural network using coupled SOA based ring lasers," IEEE Trans. Neural Netw. **13**, 1504–1513 (2002).
7. S. A. Marhon, C. J. F. Cameron, and S. C. Kremer, "Recurrent neural networks" in *Handbook on Neural Information Processing* (Springer, 2013), Vol. **49**, pp. 29–65.
8. J. Kilian and H. Siegelmann, "The dynamic universality of sigmoidal neural networks," Inform. Comput. **128**, 48–56 (1996).
9. B. A. Pearlmutter, "Gradient calculations for dynamic recurrent neural networks: a survey," IEEE Trans. Neural Netw. **6**, 1212–1228 (1995).
10. H. Jaeger and H. Haas, "Harnessing nonlinearity: predicting chaotic systems and saving energy in wireless communication," Science **304**, 78–80 (2004).
11. W. Maass, T. Natschlager, and H. Markram, "Real-time computing without stable states: a new framework for neural computation based on perturbations," Neural Comput. **14**, 2531–2560 (2002).
12. E. A. Antonelo, B. Schrauwen, and D. Stroobandt, "Event detection and localization for small mobile robots using reservoir computing," Neural Netw. **21**, 862–871 (2008).

13. P. Joshi and W. Maass, "Movement generation and control with generic neural microcircuits," in *Proceedings of BIO-AUDIT* (Springer, 2004), pp. 16–31.
14. B. Schrauwen, M. D'Haene, D. Verstraeten, and J. V. Campenhout, "Compact hardware liquid state machines on FPGA for real-time speech recognition," Neural Netw. **21**, 511–523 (2008).
15. B. Schrauwen, J. Defour, D. Verstraeten, and J. V. Campenhout, "The introduction of time-scales in reservoir computing, applied to isolated digits recognition," *Artificial Neural Networks—ICANN* (Springer, 2007), Vol. **4668**, pp. 471–479.
16. P. Buteneers, B. Schrauwen, D. Verstraeten, and D. Stroobandt, "Real-time epileptic seizure detection on intra-cranial rat data using reservoir computing," *Advances in Neuro-Information Processing* (Springer, 2013), Vol. **5506**, pp. 56–63.
17. K. Vandoorne, W. Dierckx, B. Schrauwen, D. Verstraeten, R. Baets, P. Bienstman, and J. V. Campenhout, "Towards optical signal processing using photonic reservoir computing," Opt. Express **16**, 11182–11192 (2008).
18. M. Fiers, T. V. Vaerenbergh, K. Caluwaerts, D. V. Ginste, B. Schrauwen, J. Dambre, and P. Bienstman, "Time-domain and frequency-domain modeling of nonlinear optical components at the circuit-level using a node-based approach," J. Opt. Soc. Am. B **29**, 896–900 (2012).
19. L. Larger, M. C. Soriano, D. Brunner, L. Appeltant, J. M. Gutierrez, L. Pesquera, C. R. Mirasso, and I. Fischer, "Photonic information processing beyond Turing: an optoelectronic implementation of reservoir computing" Opt. Express **20**, 3241–3249 (2012).
20. L. Appeltant, M. C. Soriano, G. V. der Sande, J. Danckaert, S. Massar, J. Dambre, B. Schrauwen, C. R. Mirasso, and I. Fischer, "Information processing using a single dynamical node as complex system," Nat. Commun. **2**, 468 (2011).
21. M. C. Soriano, S. Ortín, D. Brunner, L. Larger, C. R. Mirasso, I. Fischer, and L. Pesquera, "Optoelectronic reservoir computing: tackling noise-induced performance degradation" Opt. Express **21**, 12–20 (2013).
22. B. E. Little, S. T. Chu, H. A. Haus, J. Foresi, and J. P. Laine, "Microring resonator channel dropping filters," J. Lightwave Technol. **15**, 998–1005 (1997).
23. H. Simos, C. Mesaritakis, D. Alexandropoulos, and D. Syvridis, "Intraband cross talk properties of add–drop filters based on active microring resonators," IEEE Photon. Technol. Lett. **19**, 1649–1651 (2007).
24. H. Yi, D. S. Citrin, and Z. Zhou, "Coupling-induced high-sensitivity silicon microring intensity-based sensor," J. Opt. Soc. Am. B **28**, 1611–1615 (2011).
25. A. Pasquazi, M. Peccianti, B. E. Little, S. T. Chu, D. J. Moss, and R. Morandotti, "Stable, dual mode, high repetition rate mode-locked laser based on a microring resonator," Opt. Express **20**, 27355–27363 (2012).
26. T. V. Vaerenbergh, M. Fiers, K. Vandoorne, B. Schneider, J. Dambre, and P. Bienstman, "Towards a photonic spiking neuron: excitability in a silicon-on-insulator microring," *International Symposium on Nonlinear Theory and its Applications*, Palma, Mallorca, 2012, pp. 767–770.
27. S. Mikroulis, H. Simos, E. Roditi, and D. Syvridis, "Ultrafast all-optical AND logic operation based on FWM in a passive InGaAsP-InP microring resonator," IEEE Photon. Technol. Lett. **17**, 1878–1880 (2005).
28. A. Yariv, "Critical coupling and its control in optical waveguide-ring resonator systems," IEEE Photon. Technol. Lett. **14**, 483–485 (2002).
29. J. Niehusmann, A. Vörckel, P. H. Bolivar, T. Wahlbrink, W. Henschel, and H. Kurz, "Ultrahigh-quality-factor silicon-on-insulator microring resonator," Opt. Lett. **29**, 2861–2863 (2004).
30. C. W. Tee, K. A. Williams, R. V. Penty, and I. H. White, "Fabrication-tolerant active-passive integration scheme for vertically coupled microring resonator," IEEE J. Sel. Top. Quantum Electron. **12**, 108–116 (2006).
31. J. Yao, D. Leuenberger, M.-C. M. Lee, and M. C. Wu, "Silicon microtoroidal resonators with integrated MEMS tunable coupler," IEEE J. Sel. Top. Quantum Electron. **13**, 202–208 (2007).